



OPEN

Improved efficacy behavioral modeling of microwave circuits through dimensionality reduction and fast global sensitivity analysis

Slawomir Koziel^{1,2✉}, Anna Pietrenko-Dabrowska² & Leifur Leifsson³

Behavioral models have garnered significant interest in the realm of high-frequency electronics. Their primary function is to substitute costly computational tools, notably electromagnetic (EM) analysis, for repetitive evaluations of the structure under consideration. These evaluations are often necessary for tasks like parameter tuning, statistical analysis, or multi-criterial design. However, constructing reliable surrogate models faces several challenges, including the nonlinearity of circuit characteristics and the vast size of the parameter space, encompassing both dimensionality and design variable ranges. Additionally, ensuring the validity of the model across broad geometry/material parameter and frequency ranges is crucial for its utility in design. The purpose of this paper is to introduce an innovative approach to cost-effective and dependable behavioral modeling of microwave passives. Central to our method is a fast global sensitivity analysis (FGSA) procedure, which is devised to identify correlations between design parameters and quantify their impacts on circuit characteristics. The most significant directions identified through FGSA are utilized to establish a reduced-dimensionality domain. Within this domain, the model may be constructed using a limited amount of data samples while capturing a significant portion of the circuit response variability, rendering it suitable for design purposes. The outstanding predictive capability of the proposed model, its superiority over traditional techniques, and its readiness for design applications are demonstrated through the analysis of three microstrip circuits of diverse characteristics.

Keywords Microwave engineering, Passive circuits, Global sensitivity analysis, Behavioral modeling, Simulation-driven design, Dimensionality reduction

Computational tools have become indispensable in high-frequency electronics, among others, microwave design. These include both equivalent network simulators^{1,2}, and full-wave electromagnetic (EM) analysis^{3,4}. Versatility and reliability of the latter has been unquestionable, especially when it comes to quantifying phenomena difficult to be accounted for otherwise (EM cross-coupling, substrate anisotropy, the effects of surrounding components such as connectors, feed radiation, etc.). In particular, EM simulation is imperative for accurate evaluation of numerous modern circuits, e.g., compact structures obtained using line meandering⁵, the employment of slow-wave phenomenon^{6,7}, multi-layer implementations⁸, or defected ground structures⁹.

The downside of EM analysis is its high computational cost, which is usually acceptable for one-time design verification or limited-scope parametric studies, but becomes a bottleneck for procedures requiring massive analyses (parameter tuning^{10,11}, uncertainty quantification^{12–14}, global optimization^{15,16}, multi-criterial design^{17,18}). Globalized search is the most troublesome as it is often performed using nature-inspired algorithms^{19–24}, operating at the budgets corresponding to many thousands of system evaluations. Not surprisingly, considerable research has been focused on development of accelerated algorithms. Some of available techniques include the employment of adjoint sensitivities²⁵, sparse Jacobian updating schemes^{26–28}, parallelization²⁹, mesh deformation methods³⁰ (all of the above used to lower the expenses pertinent to sensitivity estimation in gradient-based algorithms), feature-based technology³¹, cognition-driven design³², multi-resolution techniques (e.g., space mapping³³, response correction^{34–36}), dimensionality reduction approaches³⁷, including model-order reduction^{38,39}. A growing number of approaches incorporates surrogate modelling methods^{33,40,41}, often in the

¹Engineering Optimization & Modeling Center, Reykjavik University, 101 Reykjavik, Iceland. ²Faculty of Electronics, Telecommunications and Informatics, Gdansk University of Technology, 80-233 Gdansk, Poland. ³School of Aeronautics and Astronautics, Purdue University, West Lafayette, IN 47907, USA. ✉email: koziel@ru.is

form of iterative design procedures^{42,43} (also referred to as machine learning^{44–46}). Some of popular modelling methods include polynomial regression⁴⁷, radial basis functions⁴⁸, kriging⁴⁹, support vector machines⁵⁰, Gaussian process regression (GPR)⁵¹, neural networks^{52–54}, ensemble learning⁵⁵, or polynomial chaos expansion⁵⁶.

As mentioned earlier, surrogate modelling (especially behavioral, or data-driven) is a potentially attractive way to mitigate the challenges associated with high cost of multiple EM analyses. Replacing expensive simulations with a low-cost metamodel altogether would be a desirable solution to expedite procedures such as design optimization. Nevertheless, constructing models of microwave components is a challenging task for several reasons: nonlinearity of circuit outputs, curse of dimensionality⁵⁷, and utility requirements (which entails coverage of wide geometry and material parameter ranges but also frequencies). Addressing these issues is a daunting task. Some of the methods attempt to make a better use of available data (e.g., adjust the very structure of the model to the distribution and nature of the input information, e.g., ensemble learning^{58,59}), efficiently handle large datasets (e.g., deep neural networks^{60,61}), or target a specific structure of the modeled responses (e.g., high-dimensional model representation (HDMR)⁶², orthogonal matching pursuit⁶³). On the other hand, the improvement of computational efficiency can be achieved using multi-resolution methods, for example, co-kriging⁶⁴, Bayesian model fusion⁶⁵, or two-stage GPR⁶⁶. Yet another option is performance-driven modelling^{67–70}. The techniques of this class capitalize on defining the surrogate's domain so that it covers the region encapsulating high-quality designs⁶⁷, and can be generalized to multi-resolution regime⁷¹, and employ deep learning methods⁷². The limitation is that the model setup is specific to a given set of performance specifications⁶⁸, and domain definition itself requires reference designs that need to be acquired beforehand⁶⁹. The latter increases the cost of the process. Recently, reference-design-free variations have been suggested⁷³ to mitigate this particular issue.

This research proposes a procedure for improved-efficiency generation of design-ready behavioral models of microwave passive circuits. An inherent part of our methodology is a procedure for fast global sensitivity analysis (FGSA), which has been developed to determine correlations between design parameters (both geometry and material), and establish their effects on the circuit responses. The results of FGSA allow for defining a reduced-dimensionality model domain, which is constructed using a set of directions responsible for the largest variability of the circuit responses. A rendition of a reliable data-driven model in restricted regions necessitates a limited amount of training points compared to traditional approaches. Nonetheless, the model accounts for the majority of the circuit response changes, which makes it suitable for design purposes. Comprehensive numerical studies conducted using three microstrip circuits demonstrate excellent dependability and accuracy of the proposed surrogate, and its superiority over modeling in conventional domains. The model design utility is corroborated through application case studies, in particular, circuit optimization under different scenarios concerning a variety of performance specifications.

Behavioral modeling by fast global sensitivity evaluation and dimensionality reduction

In this part of the manuscript, we elaborate on the algorithmic components of the modeling approach introduced in the study. The surrogate modeling task is stated in Section "Modelling problem statement". Section "Low-cost global sensitivity analysis" discusses a fast global sensitivity analysis (FGSA) procedure introduced to determine the relationships between design variables and frequency characteristics of the system. The latter is expressed in terms of an orthonormal set of directions, which influences the circuit responses most significantly. In Section "Domain Definition", these directions are employed to define a reduced-dimensionality domain of the behavioral model. The operation of the entire modeling framework is elucidated in Section "Complete modelling procedure".

Modelling problem statement

In the following, we mark as $R_f(\mathbf{x})$ a response of the high-fidelity circuit model, evaluated through EM analysis. Here, \mathbf{x} stands for a vector of designable parameters (cf. Table 1 for modelling-related terminology). Typically, we are interested in scattering parameters $S_{kj}(\mathbf{x}, f)$, where k and j stand for the respective circuit ports; frequency is marked as f . The goal of behavioral modeling is to render a fast replacement model (surrogate) $R_s(\mathbf{x})$ of $R_f(\mathbf{x})$, valid over the region of interest (parameter space) X . The latter is normally an interval determined by the lower and upper parameter bounds (cf. Table 1). The surrogate is supposed to represent the system responses as well as possible in a given sense. The performance metric utilized here is the relative RMS error, defined as $\|R_s(\mathbf{x}) - R_f(\mathbf{x})\| / \|R_f(\mathbf{x})\|$. The model accuracy will be estimated using the average error E_{aver} , evaluated using an independent set of testing points $\{\mathbf{x}_t^{(k)}\}_{k=1, \dots, N_t}$ and defined as

Symbol	Description	Comments
$\mathbf{x} = [x_1 \dots x_n]^T$	Vector of circuit parameters	Independent circuit dimensions to be tuned in the design process
$X = [\mathbf{u}]$	Conventional parameter space	$l = [l_1, l_n]^T$ and $\mathbf{u} = [u_1, \dots, u_n]^T$ are lower and upper bounds on parameters, i.e., we have $l_k \leq x_k \leq u_k$ for $k = 1, \dots, n$
$R_f(\mathbf{x})$	High-fidelity model	Responses of high-fidelity EM simulation model of the circuit at hand. The symbol $R_f(\mathbf{x})$ stands for aggregated circuit characteristics evaluated over the frequency range of interest F
$R_s(\mathbf{x})$	Surrogate model	Responses of the surrogate model of the circuit of interest

Table 1. Surrogate modeling of microwave components. Notation and terminology.

$$E_{aver} = \frac{1}{N_t} \sum_{k=1}^{N_t} \frac{\|\mathbf{R}_s(\mathbf{x}_t^{(k)}) - \mathbf{R}_f(\mathbf{x}_t^{(k)})\|}{\|\mathbf{R}_f(\mathbf{x}_t^{(k)})\|} \quad (1)$$

The relative error is typically more intuitive than absolute metrics because it is independent of the actual value (and the unit) of the model output. In engineering applications, the error level of a few (e.g., five) percent, typically makes the model sufficient for design purposes. A discussion of alternative error measures can be found, e.g., in^{74,75}.

Low-cost global sensitivity analysis

In Section "Introduction", we discussed some fundamental challenges encountered in the behavioral modeling of microwave components. These challenges include the curse of dimensionality, the nonlinearity of frequency characteristics, and the necessity for the model to remain valid across wide ranges of geometry and material parameters. This latter requirement is particularly crucial for practical applications, such as design optimization. Among these challenges, those associated with the number of design variables are particularly critical, as they often underpin other difficulties. Consider a scenario where the parameter space X is assumed to be uniform, meaning that typical response nonlinearity remains consistent across all regions within X . Whatever technique is employed for constructing a surrogate model (radial basis function⁴⁸, kriging⁴⁹, neural networks⁵², etc.), the modelling error is primarily a function of the mean distance between the data samples used for model training. More specifically, the smaller the distance, the better accuracy of the surrogate. The average distance, in turn, depends on the cardinality N of the dataset, and dimensionality of the space n : it is proportional to $(1/N)^{1/n}$. Note that dimensionality n plays a major role here, e.g., to reduce the average distance by a factor of two for $n=3$, the training dataset has to be enlarged by a factor of eight, whereas for $n=10$, the corresponding factor exceeds 1,000.

Thus, dimensionality reduction is critical to facilitate a reliable behavioural modelling of microwave components. One of possible approaches is variable screening, where the system variables having the least significance are identified and eliminated from the problem. Some of available techniques include the Morris method⁷⁶, Pearson correlation coefficients⁷⁷, partial or correlation coefficients⁷⁸. Another approach is global sensitivity analysis (GSA) (Sobol indices⁷⁹, Jansen method⁸⁰, regression-based methods⁸¹), the goal of which is similar, i.e., to determine the relative importance of the system parameters, and to potentially exclude those that are of minor importance. Notwithstanding, the mentioned techniques are computationally expensive: estimation of the sensitivity indicators is based on large numbers of data samples. Another issue is that for most microwave components, dropping out individual variables is not possible without impairing the system capability to reach any particular set of target operating conditions. Most parameters (including the material ones, e.g., substrate permittivity) act in synergy and affect the system characteristics through their interactions.

In this research, an alternative technique for global sensitivity analysis is developed, which is to satisfy the following requirements:

- It is cheap to execute, i.e., involves less than a hundred EM analyses of the system being modelled;
- It allows for identifying important parameter space directions rather than to determine important variables; the 'importance' is understood in terms of the effects on the circuit response variability.

The operating flow of the proposed fast GSA technique (further referred to as FGSA) has been shown in Fig. 1. The eigenvectors \mathbf{e}_j of the relocation matrix \mathbf{S} form represent the parameter space directions that have a decreasing impact on the response variability. The latter is quantified by the corresponding eigenvalues λ_j . By definition, the eigenvectors form an orthonormal basis in X . It should be mentioned that FGSA has a certain resemblance to the active subspace (AS) approaches (cf.^{82,83}). Therein, the objective is also to identify a lower-dimensionality parameter subspace corresponding to the largest response variations. However, the spectral analysis is carried out on the matrix composed of gradient vectors of the (scalar) function of interest obtained for a set of random observables. This makes AS computationally more expensive than FGSA, especially for higher-dimensional problems. On the other hand, similarly to GSA methods mentioned earlier, AS is likely to provide higher accuracy.

FGSA is employed as a tool for defining a reduced-dimensionality region for surrogate model establishment. For that purpose, we use a few most important eigenvectors, the number of which is determined as the smallest integer $N_d \in \{1, 2, \dots, n\}$ that satisfies

$$\frac{\sqrt{\sum_{j=1}^{N_d} \lambda_j^2}}{\sqrt{\sum_{j=1}^n \lambda_j^2}} \geq C_{\min} \quad (5)$$

In other words, N_d is the smallest number of vectors for which the corresponding (joint) relative least-square variability exceeds the user-defined threshold C_{\min} . In Section "Verification results", we use $C_{\min} = 0.9$; accordingly, the selected directions should account for at least ninety percent of the overall circuit response variability.

The operation of FGSA is illustrated using several examples. The first instance is a linear function $f(\mathbf{x}) = f([x_1, x_2]^T) = 3x_1 - 2x_2$, shown in Fig. 2. This function has been chosen because due to linearity, the direction of the maximum function variability can be readily identified as the gradient vector $\mathbf{g} = [3, -2]^T$. This has been confirmed by FGSA, here based on twenty random points, cf. Figure 2b. Figure 3 shows two more examples involving nonlinear functions defined so that the directions of maximum function variability can be easily assessed visually (specifically, as the vectors perpendicular to the directions of the $f(\mathbf{x})$ 'ripples'). Also in these cases, FGSA involving twenty random points correctly identified the relevant directions.

1. Input parameters:
 - Parameter space X ;
 - Computational model $\mathbf{R}_f(\mathbf{x})$;
 - Number of samples N_s ;
2. Generate N_s random vectors $\mathbf{x}_s^{(k)} \in X$, $k = 1, \dots, N_s$, preferably in a uniform manner. Here, we use modified Latin Hypercube Sampling (LHS) [83];
3. Acquire EM simulation data $\mathbf{R}_f(\mathbf{x}_s^{(k)})$, $k = 1, \dots, N_s$;
4. For each $k = 1, \dots, N_s$, find $\mathbf{x}_c^{(k)} = \mathbf{x}_s^{(j_{\min})}$ such that

$$j_{\min} = \arg \min_{\substack{1 \leq j \leq N_s \\ j \neq k}} \left\| \mathbf{x}_s^{(k)} - \mathbf{x}_s^{(j)} \right\| \quad (1)$$

In other words, $\mathbf{x}_c^{(k)}$ is the vector closest to $\mathbf{x}_s^{(k)}$ in the norm sense;

5. Compute (normalized) relocation vectors

$$\mathbf{v}_s^{(k)} = \frac{\mathbf{x}_c^{(k)} - \mathbf{x}_s^{(k)}}{\left\| \mathbf{x}_c^{(k)} - \mathbf{x}_s^{(k)} \right\|} \quad (2)$$

and the corresponding (normalized) response variabilities

$$\mathbf{r}_s^{(k)} = \frac{\mathbf{R}_f(\mathbf{x}_c^{(k)}) - \mathbf{R}_f(\mathbf{x}_s^{(k)})}{\left\| \mathbf{x}_c^{(k)} - \mathbf{x}_s^{(k)} \right\|} \quad (3)$$

for $k = 1, \dots, N_s$;

6. Define a $N_s \times n$ relocation matrix \mathbf{S} as

$$\mathbf{S} = \begin{bmatrix} \mathbf{r}_s^{(1)} (\mathbf{v}_s^{(1)})^T \\ \vdots \\ \mathbf{r}_s^{(N_s)} (\mathbf{v}_s^{(N_s)})^T \end{bmatrix} \quad (4)$$

The rows of \mathbf{S} represent relocation vectors normalized with respect to their importance in terms of how they affect the circuit response in the norm sense;

7. Perform spectral analysis of \mathbf{S} [84] in order to find its eigenvectors \mathbf{e}_j (principal components) and the corresponding eigenvalues λ_j , $j = 1, \dots, n$. The eigenvalues are ordered, so that $\lambda_1 \geq \lambda_2 \geq \dots \geq \lambda_n$.

Figure 1. Pseudocode of the proposed fast global sensitivity analysis (FGSA). The eigenvectors \mathbf{e}_j represent the parameter space directions having major effects on the circuit characteristics; the importance is quantified using the eigenvalues λ_j .

Our final example is a miniaturized microstrip coupling structure shown in Fig. 4a. The circuit features six design variables, $\mathbf{x} = [l_1 \ l_2 \ l_3 \ d \ w \ w_1]^T$. Here, FGSA is carried out based on fifty random points uniformly allocated in the design space X . The latter is determined by the lower and upper bounds $\mathbf{l} = [2.0 \ 7.0 \ 12.5 \ 0.2 \ 0.7 \ 0.2]^T$, and $\mathbf{u} = [4.5 \ 12.5 \ 22.0 \ 0.65 \ 1.5 \ 0.9]^T$. Figure 4b illustrates the EM-evaluated scattering parameters at a random parameter vector \mathbf{x} and designs perturbed along the eigenvectors identified by FGSA, $\mathbf{x} + h\mathbf{e}_k$, $k = 1, \dots, n$. As it can be observed, the response variability is the largest for $k = 1$, and gradually diminishes for increasing k .

To estimate the actual response variability, $N_r = 20$ random designs have been allocated in the parameter space, $\mathbf{x}_r^{(k)}$, $k = 1, \dots, N_r$, along with the perturbations $\mathbf{x}_r^{(k,j)} = \mathbf{x}_r^{(k)} + h\mathbf{e}_j$, $j = 1, \dots, n$. Having acquired the EM simulation data $\mathbf{R}_f(\mathbf{x}_r^{(k)})$, $k = 1, \dots, N_r$, and $\mathbf{R}_f(\mathbf{x}_r^{(k,j)})$, $k \in \{1, \dots, N_r\}$, $j \in \{1, \dots, n\}$, the variability indicators have been computed as

$$dR_j = \frac{1}{N_r} \sum_{k=1}^{N_r} \left\| \mathbf{R}_f(\mathbf{x}_r^{(k)}) - \mathbf{R}_f(\mathbf{x}_r^{(k,j)}) \right\| \quad (6)$$

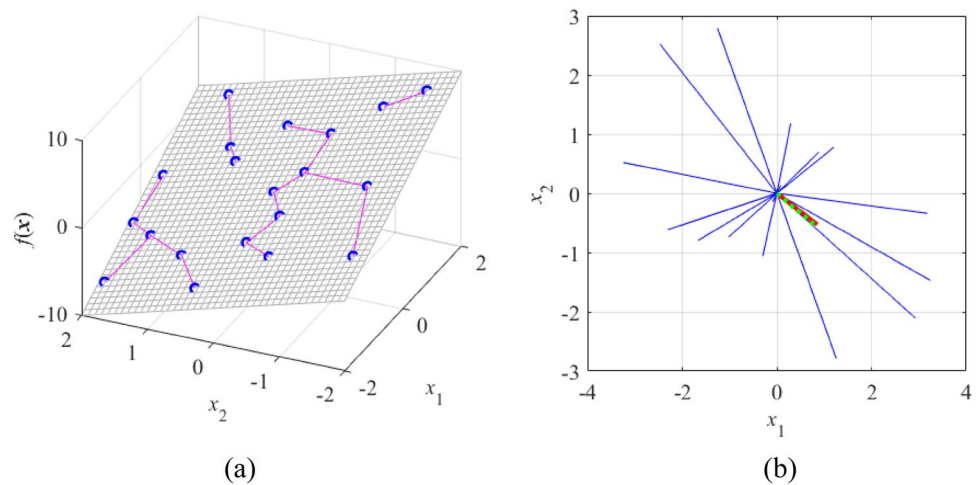


Figure 2. FGSA illustration using a linear function $f(\mathbf{x}) = f([x_1 \ x_2]^T) = 3x_1 - 2x_2$: (a) surface plot of the function (gray), twenty random observables $\mathbf{x}_s^{(k)}$ (circles), and relocation vectors $\mathbf{x}_c^{(k)} - \mathbf{x}_s^{(k)}$ (line segments); (b) relocation matrix vectors $r_s^{(k)} \mathbf{v}_s^{(k)}$ (thin lines), the largest principal component \mathbf{e}_1 (thick solid line), and the normalized gradient $\mathbf{g} = [3 \ -2]^T / 13^{1/2}$ (thick dotted line). In this example, all function variability occurs along the gradient \mathbf{g} (the function is constant in the direction orthogonal to \mathbf{g}), which is well aligned with the vector \mathbf{e}_1 , obtained using the proposed FGSA.

for $j = 1, \dots, n$. In (6), the norm $\|\mathbf{R}_f(\mathbf{x}) - \mathbf{R}_f(\mathbf{y})\|$ is computed for all circuit responses, here, the scattering parameters $S_{j1}(\mathbf{x}, f)$, $j = 1, 2, 3, 4$, and takes the form

$$\|\mathbf{R}_f(\mathbf{x}) - \mathbf{R}_f(\mathbf{y})\| = \sqrt{\sum_{j=1}^4 \int_F [S_{j1}(\mathbf{x}, f) - S_{j1}(\mathbf{y}, f)]^2 df} \quad (7)$$

where F is the simulation frequency range. The number dR_j represents an average response variability in the direction \mathbf{e}_j . Upon normalization, dR_j agree well with the normalized eigenvalues λ_j , as shown in Fig. 4(c), which demonstrates relevance of the presented sensitivity analysis approach.

Note that FGSA is computationally efficient. Many of the global sensitivity analysis techniques mentioned earlier (e.g., Sobol indices⁷⁹, regression-based methods⁸¹) require from a few hundred to a few thousands of data samples to yield accurate sensitivity assessment, depending on the problem size. FGSA is carried out based on a few dozen points. More specifically, in Section "Verification results", only fifty samples are utilized. The sensitivity estimation accuracy is somehow compromised as compared to the expensive methods, but it is sufficient of our needs. It should also be reiterated that FGSA generates a set of principal directions that generally do not coincide with the coordinate system axes. Thus, instead of eliminating individual parameters, our method enables exploration of variable interactions and their joint effects on the circuit responses.

Domain Definition

The eigenvectors \mathbf{e}_j generated by FGSA are employed to establish the model domain X_d , which is determined by N_d most significant vectors \mathbf{e}_j , $j = 1, \dots, N_d$. Recall that N_d has been determined using (5). This arrangement allows for the domain to account for the majority of the circuit response variability within X (more specifically, the fraction equal or higher than C_{\min} , cf. Section "Low-cost global sensitivity analysis"). The formal definition of the domain is

$$X_d = \left\{ \mathbf{x} \in X : \mathbf{x} = \mathbf{x}_c + \sum_{j=1}^{N_d} a_j \mathbf{e}_j \right\} \quad (8)$$

i.e., the set encapsulating parameter vectors $\mathbf{x}_c + a_1 \mathbf{e}_1 + \dots + a_{N_d} \mathbf{e}_{N_d}$, where $\mathbf{x}_c = [\mathbf{l} + \mathbf{u}]/2$ is the centre of the original domain X (cf. Table 1), and a_j , $j = 1, \dots, N_d$, are real numbers. Figure 5 provides a graphical illustration of generating X_d .

Again, while $\dim(X_d) < n$, the domain accounts for the parameter space directions that are significant for the circuit response variability. This is necessary to secure design utility of the behavioural model to be established in X_d . In this work, the underlying modelling technique is kriging⁸⁴. However, a particular choice of the modelling method unimportant: our main goal is to investigate the benefits of dimensionality reduction by means of FGSA.

Complete modelling procedure

Figure 6 showcases the modelling process pseudocode. Meanwhile, Fig. 7 illustrates the flow diagram. The procedure consists of the three major stages: (i) fast global sensitivity analysis, FGSA (Stage I), (ii) domain definition

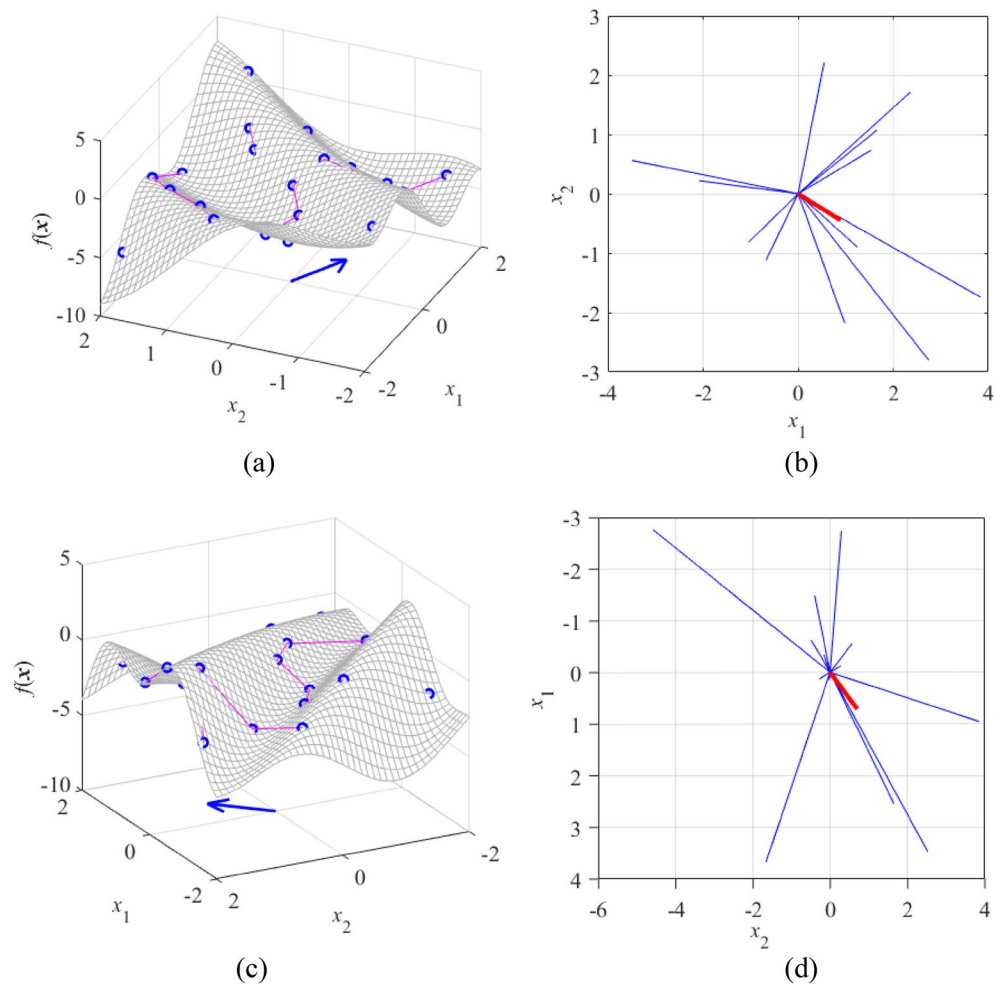


Figure 3. FGSA illustration using nonlinear functions of two variables: (a) surface plot of the first function $f_1(\mathbf{x}) = f_1([x_1 \ x_2]^T) = 2\sin(2.5x_1) - 1.5x_2 - 2\exp(x_2/5) + x_1x_2$ (gray), twenty random observables $\mathbf{x}_s^{(k)}$ (circles), and relocation vectors $\mathbf{x}_s^{(k)} - \mathbf{x}_s^{(k)}$ (line segments), as well as the principal component \mathbf{e}_1 (thick arrow); (b) relocation matrix vectors $r_s^{(k)} \mathbf{v}_s^{(k)}$ (thin lines), and the largest principal component \mathbf{e}_1 (thick solid line); (c) and (d) surface plot and relocation matrix vectors for the second function $f_2(\mathbf{x}) = f_2([x_1 \ x_2]^T) = 1.5\sin(3x_1 + 2x_2) - 1.1x_1^2 - 0.3x_2^2$. It can be noticed that the vector \mathbf{e}_1 obtained using FGSA visually corresponds to the direction associated with the highest variability of $f(\mathbf{x})$.

(Stage II), and acquisition of the training data as well as surrogate model identification (Stage III). It should be emphasized that there is only one control parameter, which is the variability threshold C_{\min} . It is set to 0.9 in the verification studies considered in Section "Verification results".

Verification results

The modeling methodology outlined in Section "Behavioral modeling by fast global sensitivity evaluation and dimensionality reduction" is validated in this section through three examples of microwave components. The modeling captures the scattering parameters of these structures across broad ranges of geometry dimensions and frequencies. Reduced-dimensionality surrogates are compared to traditional metamodels concerning both accuracy and computational cost during model setup. Additionally, we explore how the predictive power of the model scales with the size of the training dataset. The practical applicability of the proposed approach will be further discussed in Section "Application case studies".

Test cases

Validation of the modeling framework introduced in Section "Behavioral modeling by fast global sensitivity evaluation and dimensionality reduction" is realized with the help of three microwave circuits. These are:

- A miniaturized rat-race coupler (Circuit I)⁸⁵;
- A branch-line coupler using compact microstrip resonant cells (CMRCs) (Circuit II)⁸⁶;
- A dual-band equal-split power divider (Circuit III)⁸⁷.

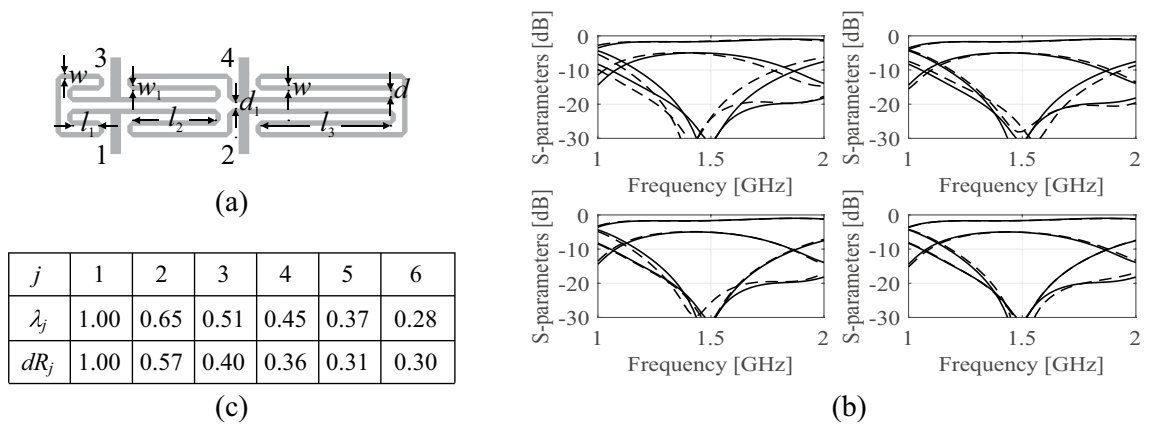


Figure 4. FGSA applied to a miniaturized rat-race coupler: (a) circuit topology, (b) scattering characteristics at a random vector \mathbf{x} and designs perturbed along the principal components, $\mathbf{x} + h\mathbf{e}_k$ (here, $h=0.1$) for the first four vectors (from top left to bottom right) obtained using FGSA, solid lines denote S -parameters at design \mathbf{x} ($|S_{11}|$ through $|S_{41}|$), whereas dashed lines denote corresponding S -parameters at the perturbed design; (c) normalized eigenvalues of the relocation matrix \mathbf{S} obtained using FSGA based on twenty random samples, as well as average EM-simulated variability indicators dR_j computed as in (6). It can be observed that response variability is gradually reduced for increasing k , which demonstrates that subsequent eigenvectors correspond to directions having less and less effect on circuit characteristics.

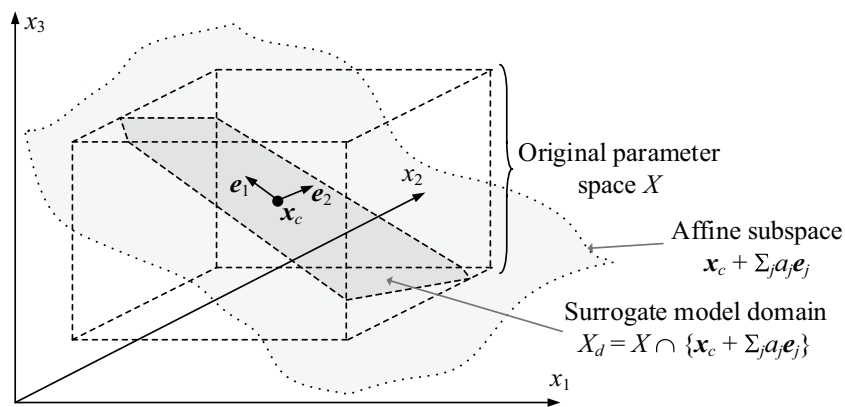


Figure 5. Constructing reduced-dimensionality domain X_d . In the example shown, the original parameter space is three dimensional, whereas X_d is determined by two principal vectors \mathbf{e}_1 and \mathbf{e}_2 . Note that X_d is a set theory intersection of X and the affine subspace $\mathbf{x}_c + \sum_{j=1,2} a_j \mathbf{e}_j$.

The architectures of the circuits have been shown in Figs. 8a, 9a, and 10a, respectively. Information about material parameters (substrate permittivity and height), design variables, parameter spaces, as well as modeled characteristics have been included in Figs. 8b, 9b, and 10b for Circuit I, II, and III. One can note that the considered modeling problems are intricate. The parameter spaces are of relatively high dimensionality (when juxtaposing them with what is typically available in the literature), whereas the parameter ranges are wide. In particular, the mean values of the ratio between upper and lower bounds is close to three for Circuit I and II, and about nine for Circuit III. Furthermore, the modeling is conducted over broad ranges of frequency (0.5 GHz to 2.5 GHz for Circuit I, 0.1 GHz to 2.5 GHz for Circuit II, and 0.5 GHz to 7.0 GHz for Circuit III). Finally, the surrogates are to represent several complex responses of each structure.

Experimental setup

The validation studies have been carried out to verify the two hypotheses concerning the properties of our modelling methodology:

- Dimensionality reduction by means of the fast GSA of Section "Low-cost global sensitivity analysis" enables a considerable enhancement of the model accuracy and scalability, i.e., more favourable relation between the training set size and the model's predictive power;
- Dimensionality reduction and the computational benefits associated with it are not detrimental to design suitability of the surrogate.

Input parameters:

- Original parameter space X (interval $[l \ u]$, where l and u are lower and upper parameter bounds, respectively);
- EM simulation model $R_f(\mathbf{x})$;
- Variability threshold C_{\min} (cf. Section 2.2).

Modelling process (Stage I: FGSA, cf. Section 2.2):

1. Generate N_s random vectors $\mathbf{x}_s^{(k)} \in X$, and acquire EM simulation data $R_f(\mathbf{x}_s^{(k)})$, $k = 1, \dots, N_s$;
2. For each $k = 1, \dots, N_s$, find $\mathbf{x}_c^{(k)} = \mathbf{x}_s^{(j_{\min})}$, $j_{\min} = \operatorname{argmin}\{1 \leq j \leq N_s, j \neq k : \|\mathbf{x}_s^{(k)} - \mathbf{x}_s^{(j)}\|\}$
3. Compute (normalized) relocation vectors $\mathbf{v}_s^{(k)} = (\mathbf{x}_c^{(k)} - \mathbf{x}_s^{(k)})/\|\mathbf{x}_c^{(k)} - \mathbf{x}_s^{(k)}\|$ and response variability factors $r_s^{(k)} = [R_f(\mathbf{x}_c^{(k)}) - R_f(\mathbf{x}_s^{(k)})]/\|\mathbf{x}_c^{(k)} - \mathbf{x}_s^{(k)}\|$, $k = 1, \dots, N_s$;
4. Define relocation matrix $\mathbf{S} = [r_s^{(1)}\mathbf{v}_s^{(1)} \ \dots \ r_s^{(N_s)}\mathbf{v}_s^{(N_s)}]^T$;
5. Find principal components (eigenvectors) \mathbf{e}_j of \mathbf{S} , and the corresponding eigenvalues λ_j , $j = 1, \dots, n$.

Modelling process (Stage II: Domain definition, cf. Section 2.3):

6. Determine domain dimensionality N_d using (5);
7. Define domain $X_d = \{\mathbf{x} \in X : \mathbf{x} = \mathbf{x}_c + \sum_{j=1, \dots, N_d} a_j \mathbf{e}_j\}$, where $\mathbf{x}_c = [l + u]/2$, and a_j , $j = 1, \dots, N_d$, are real numbers.

Modelling process (Stage III: Model identification):

8. Allocate training data in X_d , $\mathbf{x}_B^{(k)}$, $k = 1, \dots, N_B$;
9. Acquire EM data $R_f(\mathbf{x}_B^{(k)})$, $k = 1, \dots, N_B$;
10. Identify kriging interpolation model $R_s(\mathbf{x})$ using $\{\mathbf{x}_B^{(k)}, R_f(\mathbf{x}_B^{(k)})\}$, $k = 1, \dots, N_B$, as a training dataset.

Figure 6. Surrogate modelling of microwave circuits using FGSA and reduced-dimensionality surrogates.

The second hypothesis will be discussed in Section "Application case studies". Its meaning is whether operating in a reduced space leaves sufficient flexibility for surrogate to be used for design purposes. The first hypothesis will be addressed in the remaining part of this section. To investigate the features of the presented modelling approach, we compare surrogate models rendered in the full-dimensional space X with those obtained within the reduced set. The FGSA procedure is conducted based on fifty random samples allocated in X by means of modified Latin Hypercube Sampling⁸⁸. The dimensionality N_d of the model domain is computed for the threshold $C_{\min} = 0.9$ in (5), cf. Section "Low-cost global sensitivity analysis", i.e., the domain is to account for ninety percent of the system response variability or more. Furthermore, the surrogate models are established using sample sets of several sizes $N_B = 50, 100, 200, 400$, and 800. This will allow us to determine the scalability of the model predictive power as a function of N_B .

In this study, the modelling routine of choice is kriging (setup: 2nd-order polynomial as a regression function, Gaussian correlation function). However, this is of secondary importance as our goal is mainly to determine potential benefits of using FGSA and dimensionality-reduced domains. As mentioned earlier, the model accuracy is estimated using the relative root-mean square (RMS) error, $\|R_s(\mathbf{x}) - R_f(\mathbf{x})\|/\|R_f(\mathbf{x})\|$, where R_s and R_f stand for the model-predicted and EM-evaluated circuit responses. To compute the error we utilize one hundred independent test samples randomly distributed within the model domain.

Results

The first point for discussion is the sensitivity analysis of Section "Behavioral modeling by fast global sensitivity evaluation and dimensionality reduction". Table 2 includes the data on the eigenvalues λ_k generated by FGSA, and the dimensionality N_d of the model domain determined according to (5) with $C_{\min} = 0.9$. Note that in practice, N_d corresponding to variability factor slightly lower than C_{\min} was approved in order to keep the domain dimensionality as small as possible. One can observe that N_d is considerably smaller than the number n of the

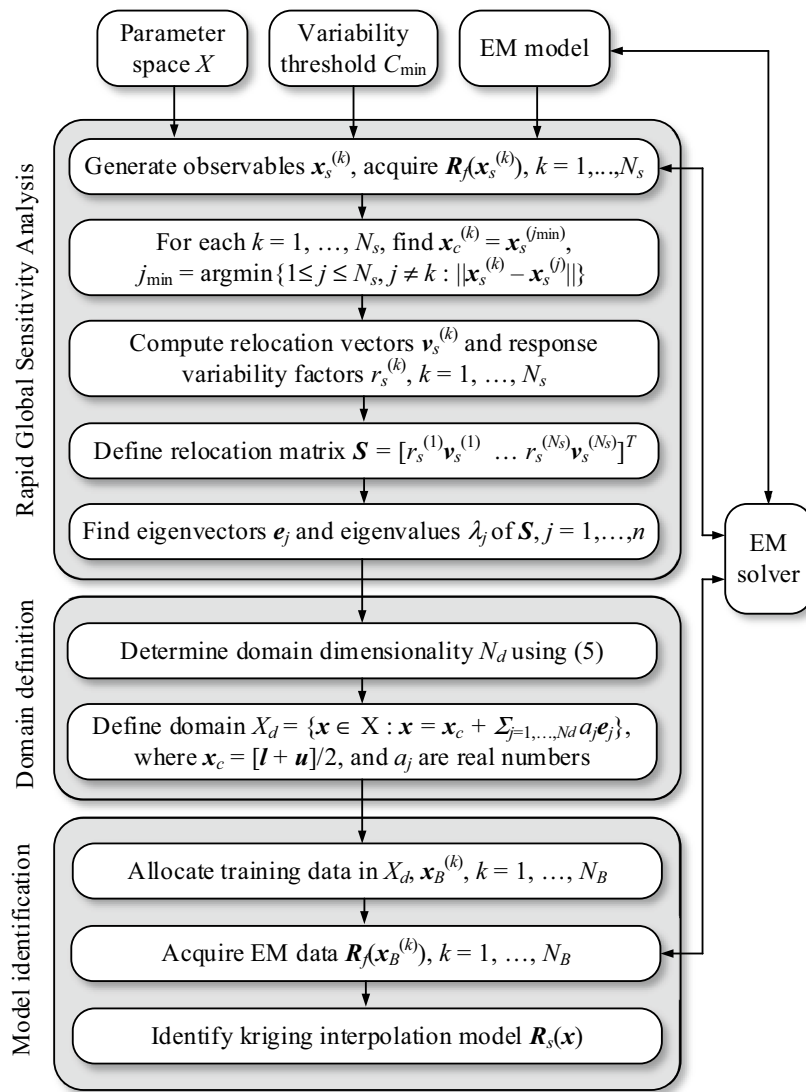
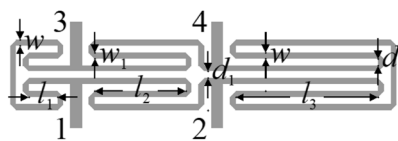


Figure 7. Flow diagram of the behavioral modeling procedure using FGSA and reduced-dimensionality domain.



Parameter	Description
Substrate	RO4003 substrate ($\epsilon_r = 3.38$, $h = 0.762$ mm)
Design parameters [§]	$\mathbf{x} = [l_1 \ l_2 \ l_3 \ d \ w \ w_1]^T$
Other parameters [§]	$d_1 = d + w - w_1 $, $d = 1.0$, $w_0 = 1.7$, $l_0 = 15$
Conventional parameter space X	$\mathbf{l} = [2.0 \ 7.0 \ 12.5 \ 0.2 \ 0.7 \ 0.2]^T$, $\mathbf{u} = [4.5 \ 12.5 \ 22.0 \ 0.65 \ 1.5 \ 0.9]^T$
Modelled characteristics	Scattering parameters S_{11} , S_{21} , S_{31} , S_{41}
Frequency range	0.5 GHz to 2.5 GHz

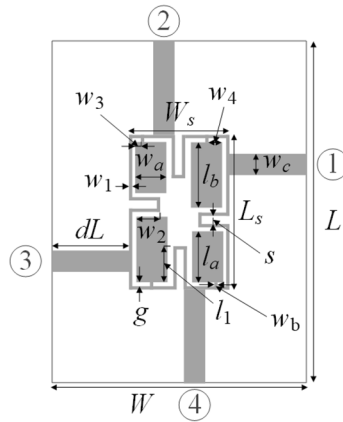
[§] Dimensions in mm.

(a)

(b)

Figure 8. Test Circuit I: (a) parameterized geometry, (b) important data.

circuit design variables. The (multiplicative) dimensionality reduction factor is 2.0 (Circuit I), 2.8 (Circuit II), and 1.8 (Circuit III). It is the smallest for Circuit III, which is the most difficult case for two reasons: (i) the modelled characteristics are defined over broad range of frequencies, and (ii) the circuit responses are highly nonlinear over the entire frequency spectrum. Furthermore, it should be emphasized that for this structure, the eigenvalues are much less reduced between λ_1 and λ_n (here, from 1.00 to 0.45), which indicates low parameter



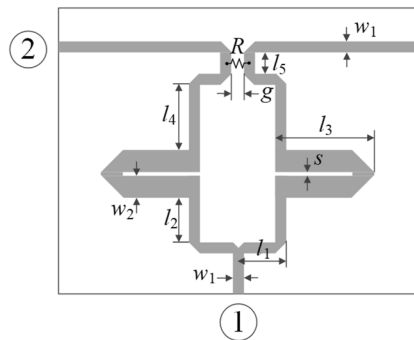
(a)

Parameter	Description
Substrate	ϵ_r – operating parameter, $h = 0.76$ mm
Design parameters ^s	$\mathbf{x} = [g \ l_1r \ l_a \ l_b \ w_1 \ w_{2r} \ w_{3r} \ w_{4r} \ w_a \ w_b]^T$ $L = 2dL + L_s, L_s = 4w_1 + 4g + s + l_a + l_b, W = 2dL + W_s, W_s = 4w_1 + 4g + s + 2w_a, l_1 = l_b l_{1r}, w_2 = w_a w_{2r}, w_3 = w_{3r} w_a, w_4 = w_{4r} w_a$
Other parameters ^s	$\mathbf{l} = [0.4 \ 0.43 \ 5.9 \ 7.7 \ 0.68 \ 0.28 \ 0.1 \ 0.1 \ 2.0 \ 0.2]^T$
Conventional parameter space X	$\mathbf{u} = [1.0 \ 0.86 \ 14.0 \ 16.5 \ 1.5 \ 0.99 \ 0.65 \ 0.25 \ 5.5 \ 0.8]^T$
Modelled characteristics	Scattering parameters $S_{11}, S_{21}, S_{31}, S_{41}$
Frequency range	0.1 GHz to 2.5 GHz

^s Dimensions in mm.

(b)

Figure 9. Test Circuit II: (a) parameterized geometry, (b) important data.



(a)

Parameter	Description
Substrate	AD250 substrate ($\epsilon_r = 2.5, h = 0.81$ mm)
Design parameters ^s	$\mathbf{x} = [l_1 \ l_2 \ l_3 \ l_4 \ l_5 \ s \ w_2]^T$
Other parameters ^s	$w_1 = 2.2$ (to ensure 50-ohm line impedance), $g = 1$
Conventional parameter space X	$\mathbf{l} = [14.5 \ 1.1 \ 13.0 \ 0.5 \ 1.6 \ 0.19 \ 3.9]^T$ $\mathbf{u} = [37.0 \ 16.6 \ 35.0 \ 15.0 \ 5.6 \ 1.5 \ 5.8]^T$
Modelled characteristics	Scattering parameters $S_{11}, S_{21}, S_{31}, S_{22}, S_{33}, S_{32}$
Frequency range	0.5 GHz to 7.0 GHz

^s Dimensions in mm.

(b)

Figure 10. Test Circuit III: (a) parameterized geometry, (b) important data.

Domain data	Circuit			
	I	II	III	
Dimensionality n of the original parameter space X	6	11	7	
(Normalized) eigenvalues of the relocation matrix S	$\lambda_1 = 1.00$	$\lambda_1 = 1.00$	$\lambda_1 = 1.00$	
	$\lambda_2 = 0.65$	$\lambda_2 = 0.66$	$\lambda_2 = 0.77$	
	$\lambda_3 = 0.51$	$\lambda_3 = 0.54$	$\lambda_3 = 0.66$	
	$\lambda_4 = 0.46$	$\lambda_4 = 0.48$	$\lambda_4 = 0.64$	
	$\lambda_5 = 0.37$	$\lambda_5 = 0.41$	$\lambda_5 = 0.50$	
	$\lambda_6 = 0.28$	$\lambda_6 = 0.39$	$\lambda_6 = 0.48$	
		$\lambda_7 = 0.30$	$\lambda_7 = 0.45$	
		$\lambda_8 = 0.25$		
		$\lambda_9 = 0.22$		
		$\lambda_{10} = 0.16$		
		$\lambda_{11} = 0.13$		
	N_d	3	4	4
Reduced-dimensionality domain [#]	$\frac{\sqrt{\sum_{j=1}^{N_d} \lambda_j^2}}{\sqrt{\sum_{j=1}^n \lambda_j^2}}$	0.89	0.88	0.88

Table 2. Fast global sensitivity analysis: eigenvalues λ_k and domain dimensionality for $C_{\min} = 0.9 \cdot N_d$ corresponding to the variability factor slightly lower than C_{\min} are accepted to maintain domain dimensionality as low as possible.

redundancy. This is in contrast to Circuits I and especially Circuit II, where the eigenvalues drop down much faster. This behaviour is typical for miniaturized components, both CMRC-based and those employing line meandering, and enables a more efficient dimensionality reduction.

The reliability of the conventional and the proposed surrogates constructed using training datasets of sizes 50 through 800 samples have been shown in Table 3. Only for Circuit III, the models were also constructed using 1,600 samples, which is because it is the most challenging case, for which it was not possible to reduce the modelling error below ten percent with the 800-sample training set. The plots of the metamodel-predicted and EM-evaluated scattering parameters of Circuit I through III for chosen test points can be found in Figs. 11, 12, and 13, respectively.

The data encapsulated in Table 3 corroborates that dimensionality reduction greatly affects the surrogate model accuracy. Circuit I is the only case where modeling in the original parameter space is capable of rendering surrogates that feature relative error below ten percent. For this structure, modeling in a reduced-dimensionality domain allows for keeping the error below five percent already for training sample sets as small as 100 samples. Circuit II is considerably more challenging. Here, the conventional model is clearly unusable (RMS error over twenty percent) even for the largest dataset. At the same time, dimensionality reduction using fast GSA enables a dramatic accuracy improvement to about six percent. Finally, for Circuit III, the most difficult case, conventional modeling is exceptionally poor, also when the training dataset cardinality is enlarged to 1,600 samples. Dimensionality reduction enables error level reduction to only eight percent, which allows us to expect that the surrogate might be usable as a design aid.

Application case studies

The numerical results presented in Section "Results" unanimously demonstrate the benefits of reducing domain dimensionality through the proposed fast global sensitivity analysis. In particular, it makes it possible to render accurate surrogate models using reasonably small numbers of training points, as shown in Figs. 11, 12, 13. Nevertheless, a more important question is whether domain restriction is not detrimental for design utility of the model. Although a dimensionality-reduced domain is smaller than the original one, recall that it is spanned along the directions that correspond to the maximum response variability (i.e., those associated with the largest

Number of training points	Model error					
	Circuit I		Circuit II		Circuit III	
	Original space X	Reduced domain X_d [this work]	Original space X	Reduced domain X_d [this work]	Original space X	Reduced domain X_d [this work]
50	25.7%	5.9%	52.3%	21.5%	63.6%	38.9%
100	17.9%	3.8%	38.3%	15.8%	53.8%	28.7%
200	13.5%	2.7%	31.0%	11.1%	45.2%	23.5%
400	9.9%	2.4%	27.3%	8.5%	40.0%	16.6%
800	8.0%	1.8%	23.3%	6.4%	35.1%	12.5%
1600	–	–	–	–	32.3%	8.4%

Table 3. Modeling results for Circuit I through III.

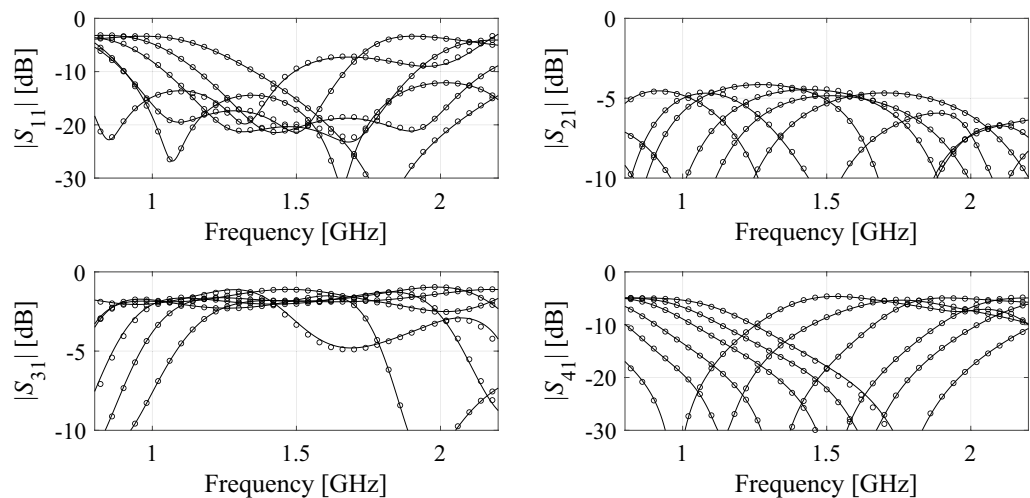


Figure 11. Circuit I: scattering parameters at the chosen testing points: EM analysis (—), and the introduced FGSA-based model (o). The training set size $N_B = 400$.

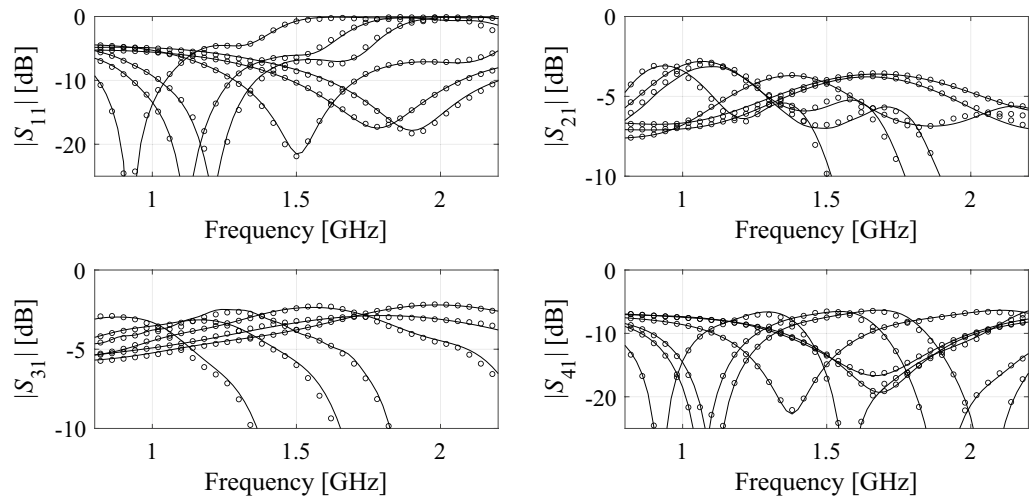


Figure 12. Circuit II: scattering parameters at the chosen testing points: EM analysis (—), and the introduced FGSA-based model (o). The training set size $N_B = 800$.

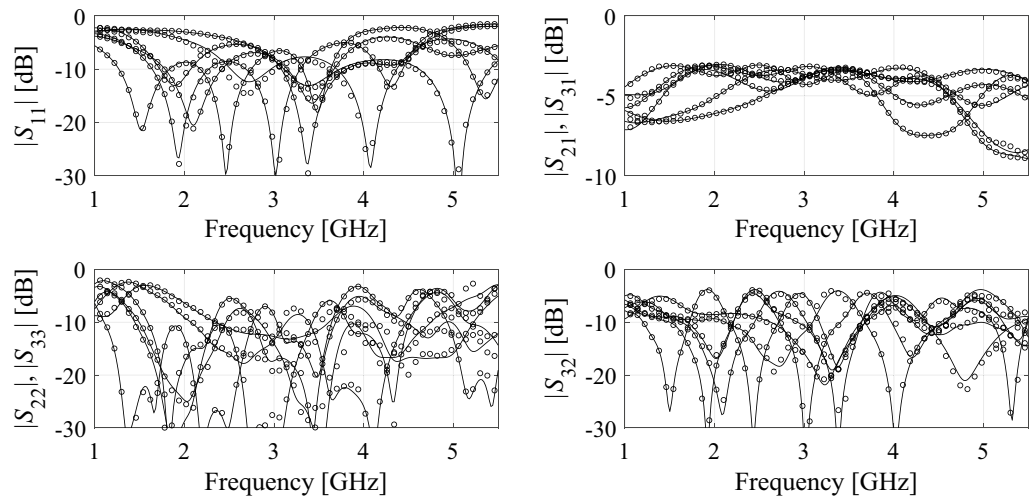


Figure 13. Circuit III: scattering parameters at the chosen testing points: EM analysis (—), and the introduced FGSA-based model (o). The training set size $N_B = 1,600$.

eigenvalues of the variability matrix \mathbf{S} of (4). Consequently, limiting the number of dimensions should not affect the ability of the surrogate to accommodate the optimum designs to a large extent. In order to verify this property, the GSA-based models are employed in this section to optimize Circuits I through III under different design scenarios. As the modeling process has been carried out over broad frequency spectra, the surrogate are utilized to optimize the respective circuit for a variety of operating frequencies, but—in the case of Circuit II—also different substrate materials (note that substrate permittivity ϵ_r is one of the design parameters for Circuit II, with the range from 2.0 to 5.0).

Table 4 delineates performance requirements for the considered devices. It should be noted that for Circuit III, equal power division is ensured by the structure's symmetry. The parameters of each circuit were tuned for four distinct target values of the operating parameters, which are f_0 and K_p for Circuit I, f_0 and ϵ_r for Circuit II, as well as f_1 and f_2 for Circuit III. The findings have been compiled in Tables 5, 6, and 7, while Figs. 14, 15, and 16 illustrate the optimized circuit responses for Circuit I, II, and III. Notably, optimization of the proposed surrogate model produces satisfactory designs across all cases. Moreover, there is excellent alignment between the model-predicted characteristics and those simulated through electromagnetic (EM) methods. These results collectively support the practical applicability of the modeling methodology discussed in this study, especially its effectiveness in designing circuits across wide ranges of operating conditions, such as center frequencies and power split ratios.

Circuit	Design objectives	Other conditions
I	1. Minimize matching $ S_{11} $ and isolation $ S_{41} $ responses at the target operating frequency f_0 ;	-
	2. Maintain target power split ratio $ S_{31} - S_{21} =Kp$ at f_0	
II	1. Minimize matching $ S_{11} $ and isolation $ S_{41} $ responses at the target operating frequency f_0 ;	Circuit implemented on substrate of relative permittivity ϵ_r^s
	2. Maintain equal power split ratio $ S_{31} - S_{21} =0$ at f_0 ;	
III	1. Minimize input matching $ S_{11} $ and output matching $ S_{22} = S_{33} $ simultaneously at the target operating frequencies f_1 and f_2 ;	-
	2. Minimize port isolation $ S_{32} $ at both f_1 and f_2 ;	
	3. Maintain equal power division ratio, i.e., $ S_{21} = S_{31} $ at f_1 and f_2	

Table 4. Design optimization scenarios for Circuits I, II, and III. ^sRelative permittivity is one of the design variables of the modelling process.

Target operating conditions			Geometry parameter values [mm]					
Case	f_0 [GHz]	K_p [dB]	l_1	l_2	L_3	d	w	w_1
1	1.0	-3	2.06	10.2	19.9	0.50	1.35	0.61
2	1.5	0	2.03	10.5	13.4	0.65	0.80	0.75
3	2.0	6	4.48	9.5	13.1	0.27	0.97	0.56
4	1.2	-3	2.50	9.5	17.7	0.38	1.19	0.51

Table 5. Circuit I: optimization results.

Target operating conditions				Geometry parameter values								
Case	F_0 [GHz]	ϵ_r	g	l_{1r}	l_a	l_b	w_1	w_{2r}	w_{3r}	w_{4r}	w_a	w_b
1	0.8	4.4	0.55	0.67	11.7	16.3	0.97	0.64	0.37	0.21	4.85	0.35
2	1.0	3.5	0.73	0.70	9.9	12.7	1.38	0.92	0.48	0.21	4.93	0.37
3	1.25	1.25	0.40	0.64	12.5	13.5	0.92	0.36	0.26	0.16	3.30	0.55
4	1.8	2.5	0.41	0.65	11.2	10.7	1.04	0.33	0.26	0.11	2.96	0.6

Table 6. Circuit II: optimization results.

Target operating conditions			Geometry parameter values [mm]						
Case	f_1 [GHz]	F_2 [GHz]	l_1	l_2	L_3	L_4	L_5	s	W_2
1	1.3	2.2	30.2	14.2	34.4	11.1	2.51	1.32	3.85
2	1.5	2.45	31.3	9.81	31.2	8.85	4.59	0.70	4.32
3	2.0	4.0	26.2	6.95	27.3	4.71	4.76	0.21	5.13
4	3.3	5.0	17.2	4.66	15.4	4.78	2.53	1.13	5.73

Table 7. Circuit III: optimization results.

Conclusion

This study presents a method for enhancing the accuracy of surrogate modeling for passive microwave components. The approach introduced is grounded in fast global sensitivity analysis (FGSA), which has been developed to identify, at a low cost, the parameter space directions that exert the most significant influence on circuit responses. By employing a small subset of these critical directions, determined through eigenvalue analysis, the surrogate model domain is effectively spanned. This setup facilitates the creation of reliable metamodels across wide frequency ranges, as well as varying geometry and material parameters, using relatively modest training

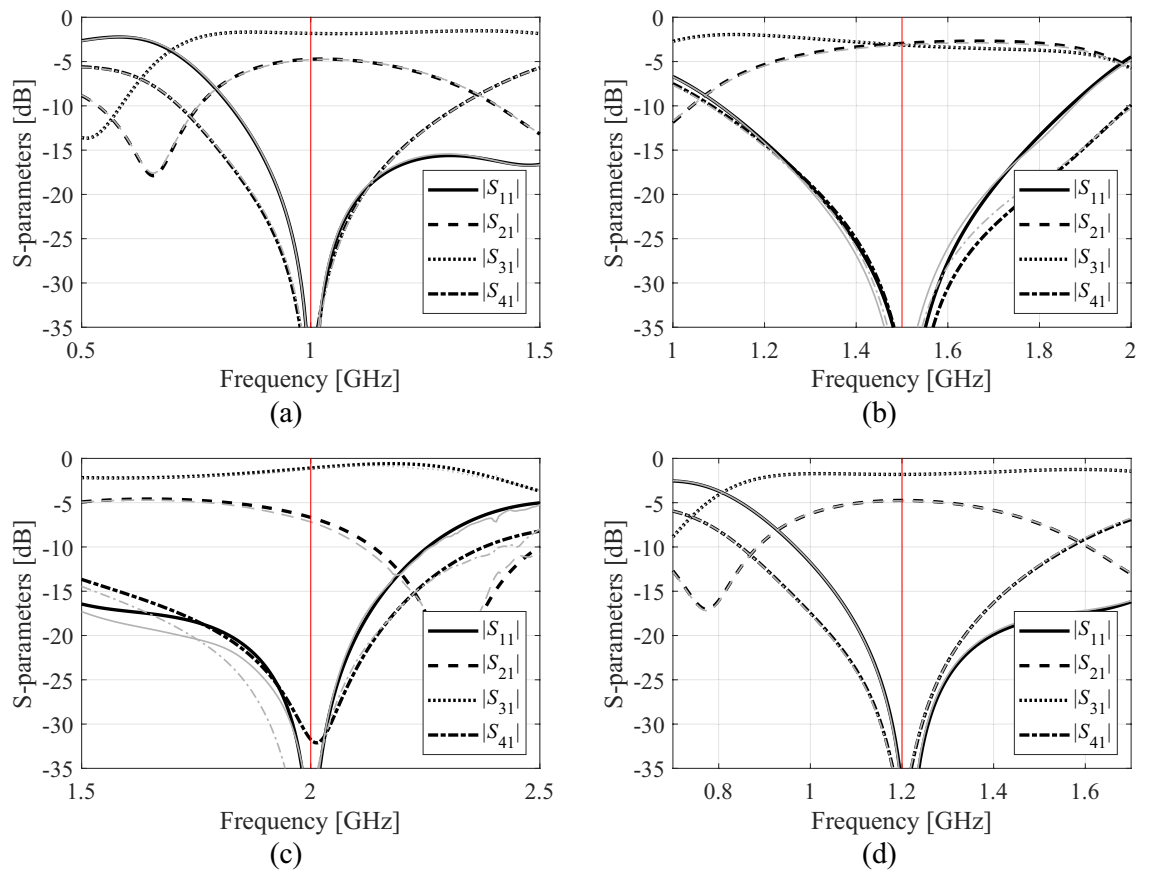


Figure 14. Optimization results for Circuit I: surrogate- (gray) and EM-simulation (black) at designs found by optimizing the proposed surrogate ($N_B = 400$). Operating frequency marked using the vertical line: (a) Case 1, (b) Case 2, (c) Case 3, (d) Case 4.

datasets. Importantly, this approach preserves the design versatility of the surrogates, as the directions defining the domain capture the majority of circuit response variability.

The proposed technique has undergone comprehensive validation using three microstrip components, including two compact couplers and a dual-band power divider. The results demonstrate a significant improvement in predictive power compared to conventional methods, with relative RMS errors reaching only a few percent even with just a few hundred training samples. This improvement is notable despite considering wide frequency ranges (0.5 GHz to 2.5 GHz, 0.1 GHz to 2.5 GHz, and 0.5 GHz to 7.0 GHz for the first, second, and third circuits, respectively) and material parameter variations (substrate permittivity ranging from 2.0 to 5.0 for the second circuit). At the same time, modeling in the original domains results in remarkably poor performance and unusable models featuring relative errors of over twenty percent (except the simplest case of a rat-race coupler).

The aforementioned investigations have been supplemented by the application case studies. In these experiments, the proposed surrogate models were employed to optimize the test circuits under a variety of scenarios (different center frequencies, power division ratios, substrate permittivity values). The obtained results allowed us to establish that dimensionality reduction as described in the paper is not detrimental to design utility of the models. The findings of this work suggest that the presented methodology may be viewed an attractive alternative to state-of-the-art modeling techniques. Although demonstrated using kriging interpolation, it can be coupled with any specific approximation method. Furthermore, it is generic as opposed to some of the recent methods, which are also domain-oriented (e.g., performance-driven techniques). Finally, it is easy to implement, which is of a practical value for researchers with less experience in the fields of numerical modeling and optimization.

It should also be emphasized that due to its data-driven nature, the proposed modelling methodology can be applied to a broader class of microwave structures. In particular, the constructed surrogate models and the dimensionality reduction process are entirely based on acquired EM simulation data. The microstrip circuits employed in Section "Application case studies" were merely illustration examples. Some of worth mentioning areas include components for 5G/6G applications (e.g., antennas operating within frequency bands beyond 24 GHz), as well as broadband systems implemented on fiberglass substrates (challenging due to geometrical complexity, position-based permittivity variations, and multi-resonance outputs).

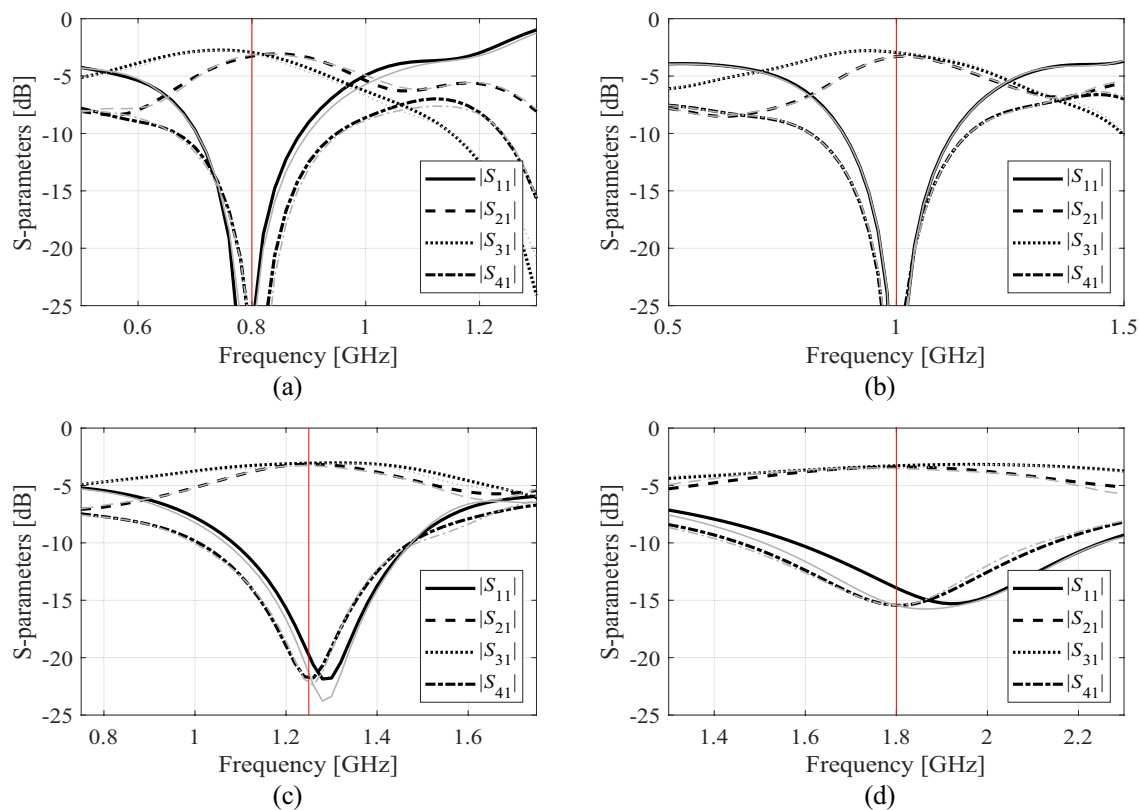


Figure 15. Optimization results for Circuit II: surrogate- (gray) and EM-simulation (black) at designs found by optimizing the proposed surrogate ($N_B=800$). Operating frequency marked using the vertical line: (a) Case 1, (b) Case 2, (c) Case 3, (d) Case 4.

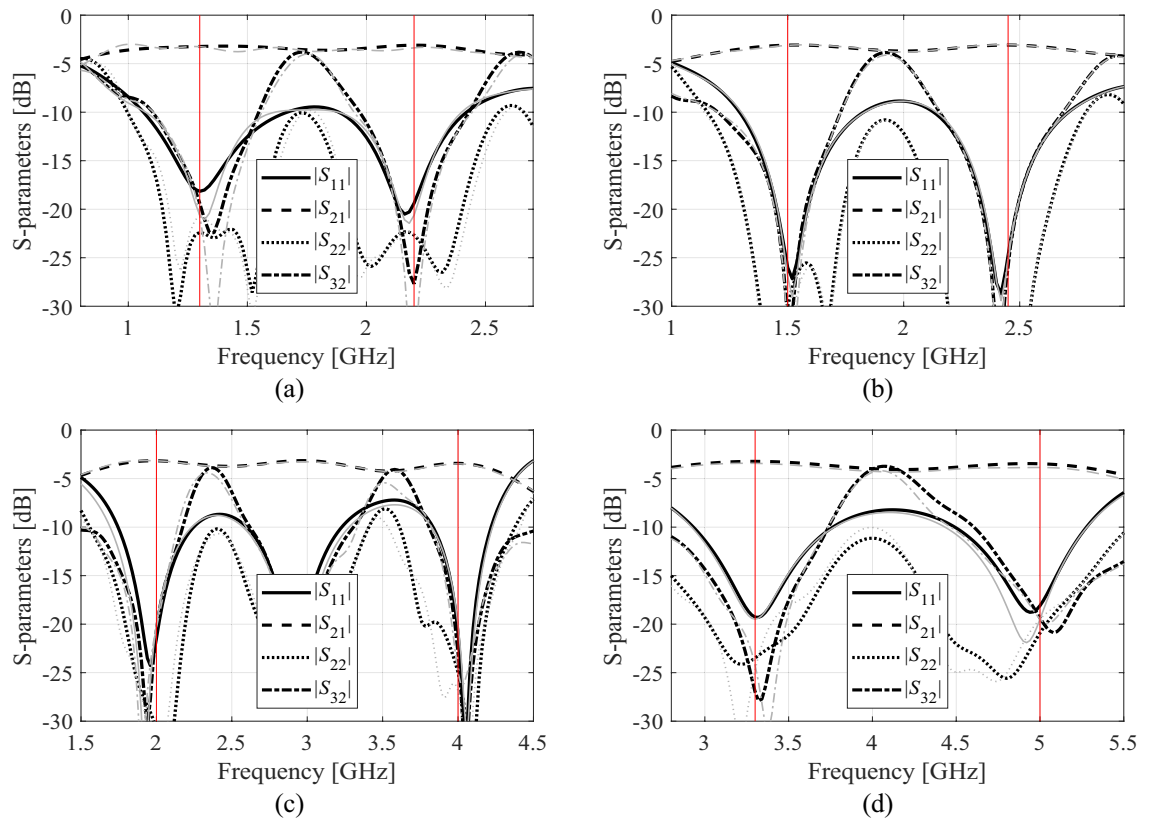


Figure 16. Optimization results for Circuit I: surrogate- (gray) and EM-simulation (black) at designs found by optimizing the proposed surrogate ($N_B=1600$). Operating frequencies marked using the vertical lines: (a) Case 1, (b) Case 2, (c) Case 3, (d) Case 4.

Data availability

The datasets used and/or analyzed during the current study available from the corresponding author on reasonable request.

Received: 29 April 2024; Accepted: 14 August 2024

Published online: 22 August 2024

References

1. ADS (Advanced Design System), Keysight Technologies, Fountaingrove Parkway 1400, Santa Rosa, CA 95403–1799, 2021.
2. AWR Microwave Office, Cadence Design Systems, Inc. San Jose, CA 95134, USA, 2022.
3. CST Microwave Studio, <https://www.3ds.com/products-services/simulia/products/cst-studio-suite/>, Dassault Systems, Rue Marcel Dassault, 78140 Velizy-Villacoublay, France, 2022.
4. HFSS, Release 19.0, ANSYS, <http://www.ansoft.com/products/hf/hfss/>, 2600 Ansys Dr., Canonsburg, PA 15317, USA, 2019.
5. Hou, Z. J. *et al.* A compact and low-loss bandpass filter using self-coupled folded-line resonator with capacitive feeding technique. *IEEE Electron Dev. Lett.* **39**(10), 1584–1587 (2018).
6. Shum, K. M., Mo, T. T., Xue, Q. & Chan, C. H. A compact bandpass filter with two tuning transmission zeros using a CMRC resonator. *IEEE Trans. Microwave Theory Techn.* **53**(3), 895–900 (2005).
7. Chen, S. *et al.* A frequency synthesizer based microwave permittivity sensor using CMRC structure. *IEEE Access* **6**, 8556–8563 (2018).
8. Wu, D.-S., Li, Y. C., Xue, Q. & Mou, J. “LTCC bandstop filters with controllable bandwidths using transmission zeros pair. *IEEE Trans. Circ. Syst. II: Express Briefs* **67**(6), 1034–1038 (2020).
9. Sen, S. & Moyra, T. “Compact microstrip low-pass filtering power divider with wide harmonic suppression. *IET Microwaves Ant. Propag.* **13**(12), 2026–2031 (2019).
10. Dong, Y., Yang, B., Yu, Z. & Zhou, J. Robust fast electromagnetic optimization of SIW filters using model-based deviation estimation and Jacobian matrix update. *IEEE Access* **8**, 2708–2722 (2020).
11. Kozziel, S., Pietrenko-Dabrowska, A. & Plotka, P. Design specification management with automated decision-making for reliable optimization of miniaturized microwave components. *Sci. Rep.* **12**, 829 (2022).
12. Ren, Z., He, S., Zhang, D., Zhang, Y. & Koh, C. S. A possibility-based robust optimal design algorithm in preliminary design state of electromagnetic devices. *IEEE Trans. Magn.* **52**(3), 7001–7504 (2016).
13. Prasad, A. K., Ahadi, M. & Roy, S. Multidimensional uncertainty quantification of microwave/RF networks using linear regression and optimal design of experiments. *IEEE Trans. Microwave Theory Techn.* **64**(8), 2433–2446 (2016).
14. Rayas-Sanchez, J. E. & Gutierrez-Ayala, V. EM-based monte carlo analysis and yield prediction of microwave circuits using linear-input neural-output space mapping. *IEEE Trans. Microwave Theory Techn.* **54**(12), 4528–4537 (2006).
15. Liu, B., Yang, H. & Lancaster, M. J. Global optimization of microwave filters based on a surrogate model-assisted evolutionary algorithm. *IEEE Trans. Microwave Theory Techn.* **65**(6), 1976–1985 (2017).

16. Torun, H. M. & Swaminathan, M. High-dimensional global optimization method for high-frequency electronic design. *IEEE Trans. Microwave Theory Techn.* **67**(6), 2128–2142 (2019).
17. Lim, D. K., Yi, K. P., Jung, S. Y., Jung, H. K. & Ro, J. S. Optimal design of an interior permanent magnet synchronous motor by using a new surrogate-assisted multi-objective optimization. *IEEE Trans. Magn.* **51**(11), 8207504 (2015).
18. Koziel, S. & Pietrenko-Dabrowska, A. Constrained multi-objective optimization of compact microwave circuits by design triangulation and Pareto front interpolation. *Eur. J. Op. Res.* **299**(1), 302–312 (2022).
19. Luo, X., Yang, B. & Qian, H. J. Adaptive synthesis for resonator-coupled filters based on particle swarm optimization. *IEEE Trans. Microwave Theory Techn.* **67**(2), 712–725 (2019).
20. Li, X., Duan, B., Zhou, J., Song, L. & Zhang, Y. Planar array synthesis for optimal microwave power transmission with multiple constraints. *IEEE Ant. Wireless Propag. Lett.* **16**, 70–73 (2017).
21. Oyelade, O. N., Ezugwu, A. E.-S., Mohamed, T. I. A. & Abualigah, L. Ebola optimization search algorithm: A new nature-inspired metaheuristic optimization algorithm. *IEEE Access* **10**, 16150–16177 (2022).
22. Majumder, A., Chatterjee, S., Chatterjee, S., Sinha Chaudhari, S. & Poddar, D. R. Optimization of small-signal model of GaN HEMT by using evolutionary algorithms. *IEEE Microwave Wireless Comp. Lett.* **27**(4), 362–364 (2017).
23. Li, X. & Luk, K. M. The grey wolf optimizer and its applications in electromagnetics. *IEEE Trans. Ant. Prop.* **68**(3), 2186–2197 (2020).
24. Ding, D., Zhang, Q., Xia, J., Zhou, A. & Yang, L. Wiggly parallel-coupled line design by using multiobjective evolutionary algorithm. *IEEE Microwave Wireless Comp. Lett.* **28**(8), 648–650 (2018).
25. Wang, J., Yang, X. S. & Wang, B. Z. Efficient gradient-based optimisation of pixel antenna with large-scale connections. *IET Microwaves Ant. Prop.* **12**(3), 385–389 (2018).
26. Koziel, S. & Pietrenko-Dabrowska, A. Reduced-cost electromagnetic-driven optimization of antenna structures by means of trust-region gradient-search with sparse Jacobian updates. *IET Microwaves Ant. Prop.* **13**(10), 1646–1652 (2019).
27. S. Koziel and A. Pietrenko-Dabrowska, “Variable-fidelity simulation models and sparse gradient updates for cost-efficient optimization of compact antenna input characteristics,” *Sensors*, **19**(8), (2019).
28. Pietrenko-Dabrowska, A. & Koziel, S. Computationally-efficient design optimization of antennas by accelerated gradient search with sensitivity and design change monitoring. *IET Microwaves Ant. Prop.* **14**(2), 165–170 (2020).
29. Zhang, W. *et al.* EM-centric multiphysics optimization of microwave components using parallel computational approach. *IEEE Trans. Microwave Theory Techn.* **68**(2), 479–489 (2020).
30. Feng, F. *et al.* Coarse- and fine-mesh space mapping for EM optimization incorporating mesh deformation. *IEEE Microwave Wireless Comp. Lett.* **29**(8), 510–512 (2019).
31. Koziel, S. Fast simulation-driven antenna design using response-feature surrogates. *Int. J. RF Micr. CAE* **25**(5), 394–402 (2015).
32. Zhang, C., Feng, F., Gongal-Reddy, V., Zhang, Q. J. & Bandler, J. W. Cognition-driven formulation of space mapping for equal-ripple optimization of microwave filters. *IEEE Trans. Microwave Theory Techn.* **63**(7), 2154–2165 (2015).
33. Cheng, Q. S., Rautio, J. C., Bandler, J. W. & Koziel, S. Progress in simulator-based tuning—the art of tuning space mapping. *IEEE Microwave Magazine* **11**(4), 96–110 (2010).
34. Koziel, S. & Unnsteinsson, S. D. Expedited design closure of antennas by means of trust-region-based adaptive response scaling. *IEEE Ant. Wireless Propag. Lett.* **17**(6), 1099–1103 (2018).
35. Su, Y., Li, J., Fan, Z. and Chen, R. Shaping optimization of double reflector antenna based on manifold mapping, *Int. Applied Comp. Electromagnetics Soc. Symp., ACES*, pp. 1–2, Suzhou, China, 1–4. (2017).
36. Koziel, S. & Leifsson, L. *Simulation-Driven Design by Knowledge-based Response Correction Techniques* (Springer, New York, 2016).
37. Pietrenko-Dabrowska, A. & Koziel, S. Reliable surrogate modeling of antenna input characteristics by means of domain confinement and principal components. *Electronics* **9**(5), 1–16 (2020).
38. Spina, D., Ferranti, F., Antonini, G., Dhaene, T. & Knockaert, L. Efficient variability analysis of electromagnetic systems via polynomial chaos and model order reduction. *IEEE Trans. Comp. Packaging Manuf. Technol.* **4**(6), 1038–1051 (2014).
39. Zhang, J., Feng, F. & Zhang, Q.-J. Rapid yield estimation of microwave passive components using model-order reduction based neuro-transfer function models. *IEEE Microwave Wireless Comp. Lett.* **31**(4), 333–336 (2021).
40. Feng, F. *et al.* Adaptive feature zero assisted surrogate-based EM optimization for microwave filter design. *IEEE Microwave Wireless Comp. Lett.* **29**(1), 2–4 (2019).
41. Hassan, A. K. S. O., Etman, A. S. & Soliman, E. A. Optimization of a novel nano antenna with two radiation modes using kriging surrogate models. *IEEE Photonic J.* **10**(4), 4800807 (2018).
42. Liu, B. *et al.* An efficient method for antenna design optimization based on evolutionary computation and machine learning techniques. *IEEE Trans. Ant. Propag.* **62**(1), 7–18 (2014).
43. Zhang, Z., Chen, H. C. & Cheng, Q. S. Surrogate-assisted quasi-Newton enhanced global optimization of antennas based on a heuristic hypersphere sampling. *IEEE Trans. Ant. Propag.* **69**(5), 2993–2998 (2021).
44. Wu, Q., Wang, H. & Hong, W. Multistage collaborative machine learning and its application to antenna modeling and optimization. *IEEE Trans. Ant. Propag.* **68**(5), 3397–3409 (2020).
45. Taran, N., Ionel, D. M. & Dorrell, D. G. Two-level surrogate-assisted differential evolution multi-objective optimization of electric machines using 3-D FEA. *IEEE Trans. Magn.* **54**(11), 8107605 (2018).
46. Wu, Q., Chen, W., Yu, C., Wang, H. and Hong, W. Multilayer machine learning-assisted optimization-based robust design and its applications to antennas and arrays, *IEEE Trans. Ant. Prop.*, Early view, (2021).
47. Chávez-Hurtado, J. L. & Rayas-Sánchez, J. E. Polynomial-based surrogate modeling of RF and microwave circuits in frequency domain exploiting the multinomial theorem. *IEEE Trans. Microwave Theory Tech.* **64**(12), 4371–4381 (2016).
48. Zhou, Q. *et al.* An active learning radial basis function modeling method based on self-organization maps for simulation-based design problems. *Knowl.-Based Syst.* **131**, 10–27 (2017).
49. de Villiers, D. I. L., Couckuyt, I. and Dhaene, T. Multi-objective optimization of reflector antennas using kriging and probability of improvement, *Int. Symp. Ant. Prop.*, pp. 985–986, San Diego, USA, (2017).
50. Cai, J., King, J., Yu, C., Liu, J. & Sun, L. Support vector regression-based behavioral modeling technique for RF power transistors. *IEEE Microwave Wireless Comp. Lett.* **28**(5), 428–430 (2018).
51. Jacobs, J. P. Characterization by Gaussian processes of finite substrate size effects on gain patterns of microstrip antennas. *IET Microwaves Ant. Prop.* **10**(11), 1189–1195 (2016).
52. Dong, J., Qin, W. & Wang, M. “Fast multi-objective optimization of multi-parameter antenna structures based on improved BPNN surrogate model. *IEEE Access* **7**, 77692–77701 (2019).
53. Calik, N., Belen, M., Mahouti, P. & Koziel, S. Accurate modeling of frequency selective surfaces using fully-connected regression model with automated architecture determination and parameter selection based on Bayesian optimization. *IEEE Access* **9**, 38396–38410 (2021).
54. Koziel, S., Mahouti, P., Calik, N., Belen, M. A. & Szczepanski, S. Improved modeling of miniaturized microwave structures using performance-driven fully-connected regression surrogate. *IEEE Access* **9**, 71470–71481 (2021).
55. Yang, J. & Wang, F. Auto-ensemble: an adaptive learning rate scheduling based deep learning model ensembling. *IEEE Access* **8**, 217499–217509 (2020).
56. Du, J. & Roblin, C. Stochastic surrogate models of deformable antennas based on vector spherical harmonics and polynomial chaos expansions: Application to textile antennas. *IEEE Trans. Ant. Prop.* **66**(7), 3610–3622 (2018).

57. Pang, Y., Zhou, B. & Nie, F. “Simultaneously learning neighborhood and projection matrix for supervised dimensionality reduction. *IEEE Trans. Neural Netw. Learn. Syst.* **30**(9), 2779–2793 (2019).
58. Müller, D., Soto-Rey, I. & Kramer, F. An analysis on ensemble learning optimized medical image classification with deep convolutional neural networks. *IEEE Access* **10**, 66467–66480 (2022).
59. Zhang, L., Ni, Q., Zhai, M., Moreno, J. & Briso, C. An ensemble learning scheme for indoor-outdoor classification based on KPIs of LTE network. *IEEE Access* **7**, 63057–63065 (2019).
60. Jin, J. *et al.* A novel deep neural network topology for parametric modeling of passive microwave components. *IEEE Access* **8**, 82273–82285 (2020).
61. Jin, J. *et al.* Deep neural network technique for high-dimensional microwave modeling and applications to parameter extraction of microwave filters. *IEEE Trans. Microwave Theory Tech.* **67**(10), 4140–4155 (2019).
62. Yücel, A. C., Bağcı, H. & Michielssen, E. “An ME-PC enhanced HDNR method for efficient statistical analysis of multiconductor transmission line networks. *IEEE Trans. Comp. Packaging Manuf. Tech.* **5**(5), 685–696 (2015).
63. Becerra, J. A. *et al.* A doubly orthogonal matching pursuit algorithm for sparse predistortion of power amplifiers. *IEEE Microwave Wireless Comp. Lett.* **28**(8), 726–728 (2018).
64. Kennedy, M. C. & O’Hagan, A. Predicting the output from complex computer code when fast approximations are available. *Biometrika* **87**, 1–13 (2000).
65. Wang, F. *et al.* “Bayesian model fusion: large-scale performance modeling of analog and mixed-signal circuits by reusing early-stage data. *IEEE Trans. Comput.-Aided Design Integr. Circ. Syst.* **35**(8), 1255–1268 (2016).
66. Jacobs, J. P. & Koziel, S. Two-stage framework for efficient Gaussian process modeling of antenna input characteristics. *IEEE Trans. Antennas Prop.* **62**(2), 706–713 (2014).
67. Koziel, S. & Pietrenko-Dabrowska, A. *Performance-Driven Surrogate Modeling of High-Frequency Structures* (Springer, New York, 2020).
68. Koziel, S. & Pietrenko-Dabrowska, A. Performance-based nested surrogate modeling of antenna input characteristics. *IEEE Trans. Ant. Prop.* **67**(5), 2904–2912 (2019).
69. Koziel, S. Low-cost data-driven surrogate modeling of antenna structures by constrained sampling. *IEEE Antennas Wireless Prop. Lett.* **16**, 461–464 (2017).
70. Koziel, S. & Sigurdsson, A. T. Triangulation-based constrained surrogate modeling of antennas. *IEEE Trans. Ant. Prop.* **66**(8), 4170–4179 (2018).
71. Pietrenko-Dabrowska, A. & Koziel, S. Antenna modeling using variable-fidelity EM simulations and constrained co-kriging. *IEEE Access* **8**(1), 91048–91056 (2020).
72. Koziel, S., Calik, N., Mahouti, P. & Belen, M. A. Accurate modeling of antenna structures by means of domain confinement and pyramidal deep neural networks. *IEEE Trans. Ant. Prop.* **70**(3), 2174–2188 (2022).
73. Koziel, S. and Pietrenko-Dabrowska, A. Knowledge-based performance-driven modeling of antenna structures, *Knowledge Based Systems*, paper no. 107698, (2021).
74. Li, X. R. & Zhao, Z. Evaluation of estimation algorithms part I: Incomprehensive measures of performance. *IEEE Trans. Aerospace Electr. Syst.* **42**(4), 1340–1358 (2006).
75. Gorissen, D., Crombecq, K., Couckuyt, I., Dhaene, T. & Demeester, P. A surrogate modeling and adaptive sampling toolbox for computer based design. *J. Mach. Learn. Res.* **11**, 2051–2055 (2010).
76. Morris, M. D. Factorial sampling plans for preliminary computational experiments. *Technometrics* **33**, 161–174 (1991).
77. Iooss, B. & Lemaitre, P. A Review on Global Sensitivity Analysis Methods. In *Uncertainty Management in Simulation-Optimization of Complex Systems* (eds Dellino, G. & Meloni, C.) 101–122 (Springer, 2015).
78. Tian, W. A review of sensitivity analysis methods in building energy analysis. *Renew. Sustain. Energy Rev.* **20**, 411–419 (2013).
79. Saltelli, A. Making best use of model evaluations to compute sensitivity indices. *Com. Physics. Comm.* **145**, 280–297 (2002).
80. Jansen, M. J. W. Analysis of variance designs for model output. *Comp. Phys. Comm.* **117**, 25–43 (1999).
81. Kovacs, I., Topa, M., Buzo, A., Rafaila, M. & Pelz, G. Comparison of sensitivity analysis methods in high-dimensional verification spaces. *Acta Technica Napocensis. Electron. Telecommun.* **57**(3), 16–23 (2016).
82. Constantine, P. G., Dow, E. & Wang, Q. Active subspace methods in theory and practice: Applications to kriging surfaces. *SIAM J. Sci. Comp.* **36**(4), 1500–1524 (2014).
83. Ma, H., Li, E. P., Cangellaris, A. C. & Chen, X. Support vector regression-based active subspace (SVR-AS) modeling of high-speed links for fast and accurate sensitivity analysis. *IEEE Access* **8**, 74339–74348 (2020).
84. Forrester, A. I. J. & Keane, A. J. Recent advances in surrogate-based optimization. *Prog. Aerospace Sci.* **45**, 50–79 (2009).
85. Koziel, S. & Sigurdsson, A. T. Performance-driven modeling of compact couplers in restricted domains. *Int. J. RF Microwave CAE* **28**(6), e21296 (2018).
86. Tseng, C. & Chang, C. A rigorous design methodology for compact planar branch-line and rat-race couplers with asymmetrical T-structures. *IEEE Trans. Microwave Theory Tech.* **60**(7), 2085–2092 (2012).
87. Lin, Z. & Chu, Q.-X. A novel approach to the design of dual-band power divider with variable power dividing ratio based on coupled-lines. *Prog. Electromagn. Res.* **103**, 271–284 (2010).
88. Beachkofski, B. and Grandhi, R. Improved distributed hypercube sampling, *American Institute of Aeronautics and Astronautics*, paper AIAA 2002–1274, 2002.

Acknowledgement

The authors would like to thank Dassault Systemes, France, for making CST Microwave Studio available. This work is partially supported by the Icelandic Centre for Research (RANNIS) Grant 239858 and by National Science Centre of Poland Grant 2022/47/B/ST7/00072

Author contributions

Conceptualization, S.K., A.P.; methodology, S.K. and A.P.; data generation, S.K. and L.L.; investigation, S.K. and A.P.; writing—original draft preparation, S.K. and A.P.; writing—review and editing, S.K. and L.L.; visualization, S.K. and L.L.; supervision, S.K.; project administration, S.K. and A.P.

Competing interests

The authors declare no competing interests.

Additional information

Correspondence and requests for materials should be addressed to S.K.

Reprints and permissions information is available at www.nature.com/reprints.

Publisher's note Springer Nature remains neutral with regard to jurisdictional claims in published maps and institutional affiliations.

Open Access This article is licensed under a Creative Commons Attribution-NonCommercial-NoDerivatives 4.0 International License, which permits any non-commercial use, sharing, distribution and reproduction in any medium or format, as long as you give appropriate credit to the original author(s) and the source, provide a link to the Creative Commons licence, and indicate if you modified the licensed material. You do not have permission under this licence to share adapted material derived from this article or parts of it. The images or other third party material in this article are included in the article's Creative Commons licence, unless indicated otherwise in a credit line to the material. If material is not included in the article's Creative Commons licence and your intended use is not permitted by statutory regulation or exceeds the permitted use, you will need to obtain permission directly from the copyright holder. To view a copy of this licence, visit <http://creativecommons.org/licenses/by-nc-nd/4.0/>.

© The Author(s) 2024